ABT737 reverses cisplatin resistance by regulating ER-mitochondria Ca²⁺ signal transduction in human ovarian cancer cells

QI XIE[1], JING SU[1], BINGXUAN JIAO[2], LUYAN SHEN[1], LIWEI MA[1], XIANZHI QU[3], CHUNYAN YU[4], XIANRUI JIANG[1], YE XU[5] and LIANKUN SUN[1]

[1]Department of Pathophysiology, Basic College of Medicine, [2]School of Public Health, Jilin University, Changchun, Jilin 130021; [3]Department of Hepatobiliary and Pancreas Surgery, The China-Japan Union Hospital, Jilin University, Changchun, Jilin 130031; [4]Department of Pathology, Basic Medical College, Beihua University; [5]Department of Histology and Embryology, Basic College of Medicine, Jilin Medical University, Jilin, Jilin 132013, P.R. China

Abstract. Bcl-2, which belongs to the Bcl-2 family, is frequently overexpressed in various types of cancer cells and contributes to drug resistance. However, the function of Bcl-2 in cisplatin resistance in human ovarian cancer cells is not fully understood. In this study, we found that the pharmacological inhibitor ABT737 or genetic knockdown of Bcl-2 increased cisplatin cytotoxicity in cisplatin-resistant ovarian cancer cells. Additionally, treatment with ABT737 or Bcl-2 siRNA increased cisplatin-induced free Ca²⁺ levels in the cytosol and mitochondria, which increased endoplasmic reticulum (ER)-associated and mitochondria-mediated apoptosis. In addition, ABT737 or Bcl-2 siRNA increased the ER-mitochondria contact sites induced by cisplatin in cisplatin-resistant SKOV3/DDP ovarian cancer cells. Consistently with the *in vitro* results, ABT737 potently synergized with cisplatin in inhibiting the growth of human ovarian cancer xenografts in nude mice. Collectively, these results indicate that pharmacological inhibitors or genetic knockdown of Bcl-2 may be a potential strategy for improving cisplatin treatment of ovarian cancer.

Correspondence to: Dr Ye Xu, Department of Histology and Embryology, Basic College of Medicine, Jilin Medical University, 5 Jilin Street, Jilin, Jilin 132013, P.R. China
E-mail: xuye_9707@163.com

Dr Liankun Sun, Department of Pathophysiology, Basic College of Medicine, Jilin University, 126 Xinmin Street, Changchun, Jilin 130021, P.R. China
E-mail: sunlk@jlu.edu.cn

Introduction

Cis-diamminedichloroplatinum (II), best known as cisplatin, is a classical chemotherapy drug that is widely used for treating advanced cancers, including ovarian cancer. The antitumor activity of cisplatin is due to its interaction with nuclear DNA, which results in the formation of DNA adducts and subsequent DNA damage-mediated apoptotic signaling (1,2). Cisplatin also has unrelated effects and accumulates in different organelles, including the endoplasmic reticulum (ER), lysosomes, and mitochondria, thus resulting in activation of apoptotic signaling pathways (3). The effect of cross-talk between different organelles on the antitumor efficacy of cisplatin has received substantial attention in recent years. The regulatory networks between the ER and mitochondria involve mitochondrial energy metabolism, lipid metabolism, Ca²⁺ signaling transmission and cell apoptosis (4). ER stress not only triggers a cascade of cellular events that lead to apoptosis but also amplifies the apoptotic signal. ER stress enhances the mitochondrial apoptosis pathway via highly efficient transportation of Ca²⁺ from the ER to the mitochondria (5). Hence, studying the cellular mechanisms underlying the signaling between the ER and mitochondria should provide new insights into cisplatin resistance in ovarian cancer.

The ER is a central membrane-bound organelle that is the main Ca²⁺ storage compartment in most cell types and has an extremely important role in maintaining Ca²⁺ homeostasis. The large release of Ca²⁺ from the ER, an early event in cell apoptosis, results in cytosolic and mitochondrial Ca²⁺ overload (6). Calpains are a complex family of Ca²⁺-dependent cysteine proteases that cleave various protein substrates. The ubiquitous calpain isoforms can be divided into calpain-1 (μ-calpain) and calpain-2 (m-calpain) according to the cytosolic Ca²⁺ concentration (μM or mM range) required for their activation (7). Recent research has shown that calpain plays a key role in ER stress-mediated apoptosis and mitochondria-mediated

apoptosis (8-10). Huang *et al* have reported that the ER stress inducer thapsigargin (TG) increases intracellular Ca^{2+} levels and subsequently activates calpains; this activation is followed by the subsequent activation of caspase-3 and caspase-9 and the induction of CHOP. As expected, EGTA and BAPTA-AM, intracellular Ca^{2+} chelators, inhibit the TG-induced activation of the calpains, caspase-3, and caspase-9 and suppress the TG-induced CHOP protein in hepatic stellate cells (8). Interestingly, after silencing calpain-1 and calpain-2, researchers have demonstrated that calpain-1 (but not calpain-2) triggers ER stress in an *in vitro* model of hypoxia/reoxygenation (10). However, the relationship between calpains and ER-mitochondria interactions remains unclear. Ca^{2+} can also be taken up by the mitochondria through the mitochondrial calcium channel uniporter (MCU), which causes mitochondrial depolarization, thereby contributing to the opening of the permeability transition pore (PTP) and altering the permeability of the inner membrane of the mitochondria (IMM). The PTP can further lead to mitochondrial swelling and mitochondrial outer membrane permeabilization (MOMP), with a consequent release of Cyto C and caspase-activating factors and the induction of cell apoptosis (11). In our previous study, using the cytoplasmic Ca^{2+}-indicating fluorophore Fluo-4/AM and the mitochondrial Ca^{2+}-indicating fluorophore Rhod-2/AM, we found that cisplatin causes pro-apoptotic Ca^{2+} release from the ER to the cytosol and mitochondria, thus leading to cytosolic and mitochondrial Ca^{2+} overload, which contributes to ER-mediated apoptosis and mitochondria-mediated apoptosis in cisplatin-sensitive SKOV3 ovarian cancer cells (12). These results have confirmed that a large release of Ca^{2+} from the ER to the cytosol and mitochondria is very important for ER-mediated apoptosis and mitochondrial apoptosis. However, the exact mechanism by which the cisplatin-induced ER Ca^{2+} release enters the mitochondria is not known.

In eukaryotic cells, intracellular organelles determine cell fate and maintain cellular homeostasis through their physical interactions with one another; the functional or physical interaction between mitochondria and the ER (referred to as mitochondria-associated ER membranes, MAM) is a prime example (13,14). MAM serves to establish close communication between the mitochondria and ER, including efficient transportation of Ca^{2+} from the ER to the mitochondria. The subcellular compartment and function of MAM is under intense investigation because it is increasingly recognized as an important region controlling cell physiology. In the MAM, Ca^{2+} release has been proposed to occur through the ER Ca^{2+} channel inositol 1,4,5-trisphosphate receptor (IP3R, the major ER Ca^{2+} release channel) to voltage-dependent anion channel 1 (VDAC1, the main mitochondrial Ca^{2+} uptake pathway) on the outer mitochondrial membrane (OMM) (13). Glucose-regulated protein 75 (Grp75) and mitofusin 2 (Mfn2), known as molecular bridges, help to increase ER-mitochondria contact sites (15). Electron microscopy and fluorescence microscopy, two important technologies, have been widely used to observe the regions of close contacts between the ER and mitochondria (16). Moreover, Wieckowski *et al* have provided a detailed introduction on the optimized protocols to isolate MAM fraction from tissues and cells (17). By adapting the protocol, Paillard at the Université de Montpellier and his colleagues have found that lethal hypoxia-reoxygenation contributes to H9c2 cell injury accompanied by a significant increase in Grp75 in the MAM, which indicates increased ER and mitochondria physical interactions. Using Rhod-2/AM loading, they have also shown that increased ER and mitochondrial interactions lead to lethal reperfusion injury through mitochondrial Ca^{2+} overload (18). Guo *et al* have shown that overexpression of Mfn2 enhances H_2O_2-induced vascular smooth muscle cell apoptosis, perhaps through excessive ER-mitochondria tethering and Ca^{2+} transfer (19). These results suggest that there is a positive correlation between MAM and cell apoptosis. However, it is unclear whether there is a link between MAM and cisplatin resistance in ovarian cancer. Although a number of indicators suggest that MAM may be useful in cancer treatment, the potential of MAM in cancer treatment has not been studied systematically. Hence, it is very important to explore the effects of MAM on cisplatin-induced cell apoptosis to clarify the mechanism of cisplatin resistance.

A systematic survey of the transcriptional profiles of various cancer cell types has indicated that the dysregulation of Bcl-2 is a key distinguishing factor between normal and cancer cells. Additionally, empirical evidence has shown a positive correlation between Bcl-2 expression and cisplatin resistance in cancer cells (20). In our previous studies, we have demonstrated that Bcl-2 expression in cisplatin-resistant SKOV3/DDP cells is significantly higher than that in cisplatin-sensitive SKOV3 cells (21). During ER stress, by interacting with the IP3R, Bcl-2 and Bcl-xL have been shown to decrease the ER Ca^{2+} load, thereby preventing excessive pro-apoptotic Ca^{2+} signals and mitochondrial Ca^{2+} overload, and finally to inhibit cell apoptosis (22). High expression of Bcl-2 also results in partial VDAC closure, which is accompanied by a marked decrease in mitochondrial Ca^{2+} levels (23). Interestingly, by analyzing MAM composition in Chinese hamster ovary cells, Meunier and Hayashi have demonstrated that Bcl-2 is enriched at the MAM (24). However, the exact role of Bcl-2 in cisplatin-induced SKOV3/DDP cell apoptosis remains unknown. ABT-737, a potent small-molecule inhibitor of Bcl-xL and Bcl-2, can bind to the hydrophobic groove in Bcl-2 and Bcl-xL and consequently prevent them from sequestering proapoptotic BH3-only protein. ABT737 exhibits synergistic cytotoxicity and induced significant apoptosis in various cancer types, including ovarian, lung and bladder cancers (25). Moreover, ABT737 has been reported to enhance the cisplatin-induced apoptosis in cancer cells (25). Hence, we propose that ABT737 reverses cisplatin resistance by regulating ER-mitochondria Ca^{2+} signal transduction in human ovarian cancer cells.

Materials and methods

Antibodies and drugs. Anti-caspase-3 (sc-7272), anti-caspase-4 (sc-56056), anti-cleaved caspase-4 (sc-22173-R), and anti-caspase-9 (sc-56073) antibodies (Abs) were purchased from Santa Cruz Biotechnology (Santa Cruz, CA, USA). Anti-cleaved caspase-3 (ab2302), anti-cleaved caspase-9 (ab2324), anti-PDI (ab2792), anti-VDAC1 (ab14734), anti-CHOP (ab11419), anti-IP3R (ab5804) Abs were purchased from Abcam Ltd. (Hong Kong, China). Anti-β-actin (60008-1-Ig), anti-Bax (50599-2-Ig), anti-Bcl-2 (12789-1-AP), anti-cytochrome *c* (Cyto C) (10993-1-AP), anti-Grp78/BIP (11587-1-AP), anti-

Grp75 (14887-1-AP), anti-mitofusin 2 (Mfn2) (12186-1-AP), anti-β-tubulin (10068-1-AP), anti-calreticulin (10292-1-AP), peroxidase-conjugated AffiniPure goat anti-mouse IgG (H+L) (SA00001-1), peroxidase-conjugated AffiniPure goat anti-rabbit IgG (H+L) (SA00001-2) and anti-IgG control (30000-0-AP) Abs were purchased from Proteintech Group, Inc. (Chicago, IL, USA). The anti-calpain-1 catalytic subunit (#31038-1) Ab was purchased from SAB (College Park, MD, USA). Cisplatin was purchased from Sigma-Aldrich (St. Louis, MO, USA) and dissolved in normal saline (NS) for *in vitro* use and animal studies. ABT-737 was provided by Abbott Laboratories (Abbott Park, IL, USA) and dissolved in dimethyl sulfoxide (DMSO) for *in vitro* use and animal studies. 2-aminoethyl diphenylborinate (2-APB) (ab120124) was purchased from Abcam Ltd.

Cell culture. The cisplatin-resistant clone SKOV3/DDP was obtained from the Peking Union Medical College (Beijing, China). COC1/DDP and A2780/DDP cells were purchased from the American Type Culture Collection (Manassas, VA, USA). SKOV3/DDP, COC1/DDP and A2780/DDP cells were maintained in IMDM (Gibco; Thermo Fisher Scientific, Inc., Carlsbad, CA, USA), supplemented with 10% (v/v) fetal calf serum (Gibco; Thermo Fisher Scientific, Inc.), 100 mg/ml streptomycin and 100 U/ml penicillin (each from Genview, Galveston, TX, USA). The cells were incubated at 37°C in an atmosphere containing 5% CO_2.

Cell viability assay. Cell viability was determined using a 3-(4,5-dimethylthiazol-2-yl)-2,5-diphenyltetrazolium bromide (MTT) assay (Beyotime Institute of Biotechnology, Haimen, China). The cisplatin-resistant ovarian cancer cells, during the exponential growth phase, were seeded into 96-well culture plates in 100 μl of IMDM at a density of 1.0×10^4 cells/well. After a 24-h incubation, the indicated drugs were added for another 24 h in four parallel wells. The MTT assays were performed as follows: 20 μl of MTT solution [5 mg/ml in phosphate-buffered saline (PBS)] was added to each well, and the cells were incubated at 37°C for 4 h. At the end of the incubation, 150 μl of DMSO (Beijing Chemical Industry Co., Ltd., Beijing, China) was added to each well. The cells were agitated for 10 min prior to measuring the absorbance at 570 nm using a model 680 microplate reader (Bio-Rad Laboratories, Inc., Hercules, CA, USA). The growth inhibition rate was calculated as follows: Inhibition (%) = [1 - (absorbance of experimental group / absorbance of control group)] x 100. The mean value of four replicate wells was calculated for each treatment group.

Annexin V and cell death assay. The Muse™ Annexin V Dead Cell kit (Ref. MCH 100105, Merck Millipore, Darmstadt, Germany) was used to monitor cell death. Exponentially growing cisplatin-resistant ovarian cancer cells were seeded into 6-well culture plates at a density of 2×10^5 cells/well. After exposure to different experimental conditions, the cells were trypsinized and resuspended in IMDM with 10% FBS at a concentration of 1×10^6 cells/ml. Cells were incubated with Annexin V and Dead Cell reagent in a dark room at room temperature for 20 min. Finally, the samples were measured by flow cytometry (Muse Cell Analyzer, Merck Millipore).

Mitochondrial membrane potential ($\Delta\Psi m$). Changes in the mitochondrial membrane potential ($\Delta\Psi m$) during the early stages of apoptosis were assayed using the Muse MitoPotential assay (Ref. MCH 100110, Merck Millipore) in SKOV3/DDP cells treated with cisplatin alone or in combination with ABT737. Briefly, cells were harvested, and the cell pellet was suspended in assay buffer (1×10^5 cells/100 μl). MitoPotential dye working solution was added, and the cell suspension was incubated at 37°C for 20 min. After the addition of Muse MitoPotential 7-AAD dye (propidium iodide) and incubation for 5 min, changes in $\Delta\Psi m$ and in cellular plasma membrane permeabilization were assessed on the basis of the fluorescence intensities of both the dyes, which were analyzed by flow cytometry (Muse Cell Analyzer, Merck Millipore).

Immunoblotting. Whole cell protein extracts from SKOV3/DDP cells were prepared with cell lysis buffer (50 mM Tris-HCl, pH 7.5, 150 mM NaCl, 1 mM Na_2EDTA, 1 mM EDTA, 1% Triton, 2.5 mM sodium pyrophosphate, 1 mM β-glycerophosphate, 1 mM Na_3VO_4, 1 mM NaF, 1 μg/ml leupeptin, and 1 mM PMSF) for western blotting. The protein extracts were quantified using a Bio-Rad kit (Pierce). Then, the protein extracts were resolved by 10% SDS-PAGE and transferred to a PVDF membrane (GS0914, Millipore). After being blocked in 5% non-fat milk in buffer [10 mM Tris-HCl (pH 7.6), 100 mM NaCl and 0.1% Tween-20], the membranes were probed with primary antibodies at 37°C for 2 h. The membranes were then incubated with HRP-conjugated secondary antibodies at room temperature for 1.5 h. Immunodetection was performed using enhanced chemiluminescence reagents (Thermo Scientific, Rockford, IL, USA), and images were captured using a Syngene Bio Imaging System (Synoptics, Cambridge, UK). Specific proteins were quantified by densitometry using Quantity One software (Bio-Rad Laboratories), normalized to actin, and presented as the mean ± SD of three independent experiments.

Calcium concentration analysis. The cytoplasmic Ca^{2+}-sensitive fluorescent dye Fluo-4/AM (Molecular Probes) and the mitochondrial Ca^{2+}-sensitive fluorescent dye Rhod-2/AM (AAT Bioquest, Sunnyvale, CA, USA) were used to measure the Ca^{2+} concentration according to the manufacturer's instructions. Before exposure to different experimental conditions, the cells were incubated with Fluo-4/AM or Rhod-2/AM for 30 min at 37°C. Cell samples were then analyzed by confocal laser microscopy. All experiments were performed in triplicate.

Immunofluorescence staining and confocal laser microscopy. Cells were seeded onto coverslips in 24-well plates at a density of 5×10^4 cells/well and allowed to recover overnight. After treatment with the indicated drugs, cells were washed three times with cold 0.1 M PBS and fixed in 4% (w/v) paraformaldehyde/PBS for 20-30 min, stained with the nuclear stain Hoechst 33342/H_2O (2 μg/ml, Sigma) for 30 min, washed with 0.01 M PBS, and examined using Olympus FV1000 confocal laser microscopy to reveal chromatin condensation. The co-localization of IP3R and VDAC1 and the expression of PDI were examined by the indirect immunofluorescence method. Cells were cultured on coverslips overnight, then treated with the indicated drugs, and rinsed with 0.1 M

PBS three times. After incubation, the cells were fixed with 4% paraformaldehyde for 20 min, permeabilized with 0.1% Triton X-100 (Sigma-Aldrich) for 5 min, washed three times with 0.01 M PBS, and then blocked for 30 min in 5% (w/v) non-immune animal serum (goat) (Beyotime Biotechnology, Shanghai, China) PBS, and incubated with primary antibody (IP3R, VDAC1, PDI) overnight at 4°C. The next day, the slides were incubated with the Alexa Fluor-488/546-conjugated secondary antibody (1:400 dilution; Invitrogen) for 1 h, then stained with Hoechst 33342 (2 μg/ml) for 2 min, and washed three times with PBS. After mounting, the cells were examined by Olympus FV1000 confocal laser microscopy.

Subcellular fractionation. The purification of the cytoplasmic fraction, ER fraction, pure mitochondrial fraction, crude mitochondrial fraction and the MAM fraction were performed as previously described (17). The above fractions were lysed in RIPA buffer [1% sodium deoxycholate, 0.1% SDS, 1% Triton X-100, 10 mM Tris (pH 8.0), 0.14 M NaCl] for immunoblotting with antibodies against IP3R, VDAC1, Bcl-2, calreticulin, Cyto C, Mfn2, Grp75 and tubulin. For co-immunoprecipitation analysis, the MAM lysates were pre-cleared with protein G agarose beads (Proteintech Group, Inc.) for 1 h at 4°C. Then, equal amounts of sample lysates were incubated with either 2 μg of IgG or anti-IP3R antibody for 20 h at 4°C, and this was followed by precipitation with protein G agarose beads. Immunoprecipitated proteins from MAM lysates and total MAM lysates were subjected to immunoblot analysis with the anti-IP3R antibody and anti-VDAC1 antibody. Total MAM lysates were used as the input control. The results are representative of three independent experiments.

Electron microscopy. Electron microscopy and morphometric analysis were performed as described previously (26). Cells were fixed for 30 min with ice-cold 2.5% glutaraldehyde in 0.1 M cacodylate buffer, embedded in Epon, and processed for transmission electron microscopy by standard procedures. Representative areas were chosen for ultra-thin sectioning and examined on a transmission electron microscope at a magnification of x20,000.

Bcl-2 knockdown by small interfering RNA. Small interfering RNA (siRNA) sequences targeting human Bcl-2 and a non-target sequence were constructed by Genechem (Shanghai, China). The Bcl-2 siRNA sequence was CCG-CAT-TTA-ATT-CAT-GGT-ATT and that of the non-target siRNA (Scramble) was TTC-TCC-GAA-CGT-GTC-ACG-T. Transfections with the siRNAs were performed using Lipofectamine 2000 (Invitrogen, Carlsbad, CA, USA) according to the manufacturer's protocol. Briefly, cisplatin-resistant SKOV3/DDP cells were placed into 6-well plates and transfected the next day with 4 μg of Bcl-2 siRNA or siScramble, using 10 μl of Lipofectamine 2000 (at 1 μg/μl). Cells were harvested 2 days after transfection; whole cell lysates were isolated for western blots. For MTT assays, transfected cells were treated with cisplatin for 24 h, and then subjected to the MTT assay to determine cell viability.

Human tumor xenografts. BALB/c nude mice (4-6 weeks old) were purchased from Beijing Vital River Laboratory Animal Technology Co. Ltd., China. Animals were maintained in specific pathogen-free conditions and a controlled light and humidity environment. Animal experiments were conducted in accordance with the National Institutes of Health Guide for the Care and Use of Laboratory animals. SKOV3/DDP cells (5x10^6) were subcutaneously injected into the right flank of each mouse. Tumor volume (mm^3) was measured every 4 days using a Vernier caliper and calculated as 0.4 x (short length)^2 x long length. Treatment was initiated when tumors reached a volume of 45-55 mm^3 (day 16). The mice were randomly divided into 4 groups (5 animals/group) and received NS (IP, daily), 4 mg/kg cisplatin (IP, every other day), 50 mg/kg ABT737 (IP, every other day), or a combination treatment for 20 days. The mice were sacrificed, and the experiment was terminated at the end of 36 days. Tumors were isolated, weighed, and imaged.

Immunohistochemistry. Immunohistochemical staining for cleaved caspase-3 was performed on 5-μm thick sections embedded in paraffin after formalin fixation. The sections were de-paraffinized in xylene and rehydrated in graded ethanol solutions (reducing concentration from 95 to 70%). The sections were incubated in H$_2$O$_2$ solution (3% H$_2$O$_2$ in PBS buffer) for 30 min to block endogenous peroxidase activity. Antigen retrieval was performed in retrieval buffer (pH 9.0, 20 mM Tris, 0.05 mM EDTA, 0.05% Tween-20 buffer) in a 99°C bath for 20 min. The sections were subsequently incubated at 4°C overnight with anti-cleaved caspase-3. After rinsing with PBS buffer, the secondary antibody (MaxVision™ HRP-Polymer Anti-Rabbit IHC kit, Maixin Bio, China) was applied for 15 min at RT. The DAB (Maixin Bio, China) solution was used as the chromogen. Finally, the sections were counterstained with hematoxylin (Sigma) to identify the nuclei. The images were observed and analyzed using a microscope (Leica DM 4000B) with Image-Pro Plus 6.0 software.

Terminal deoxynucleotidyl transferase dUTP nick-end labeling (TUNEL). Apoptosis analysis was performed using an In Situ Cell Death Detection kit (Roche, Indianapolis, IN, USA) to identify DNA breaks according to the manufacturer's instructions. Sections were incubated with TUNEL reaction mix containing 10 U of terminal deoxyribosyltransferase, 10 mM dUTP biotin, and 2.5 mM cobalt chloride in 1X terminal transferase reaction buffer for 1 h at 37°C in a humidified atmosphere. The DAB (Maixin Bio, China) solution was used as the chromogen. Finally, the sections were counterstained with hematoxylin (Sigma) to identify the nuclei. The images were observed and analyzed using a microscope (Leica DM 4000B) with Image-Pro Plus 6.0 software.

Statistical analyses. All values are presented as mean ± SEM. Statistical analysis was performed using one-way analysis of variance (ANOVA) followed by the Bonferroni multiple comparison test with the software GraphPad Prism version 6.00 for Mac (GraphPad Software, La Jolla, CA, USA). A value of P<0.05 was considered statistically significant.

Results

ABT737 increases cisplatin-induced growth inhibition and apoptosis in cisplatin-resistant ovarian cancer cells. We treated cisplatin-resistant ovarian cancer cells (SKOV3/DDP,
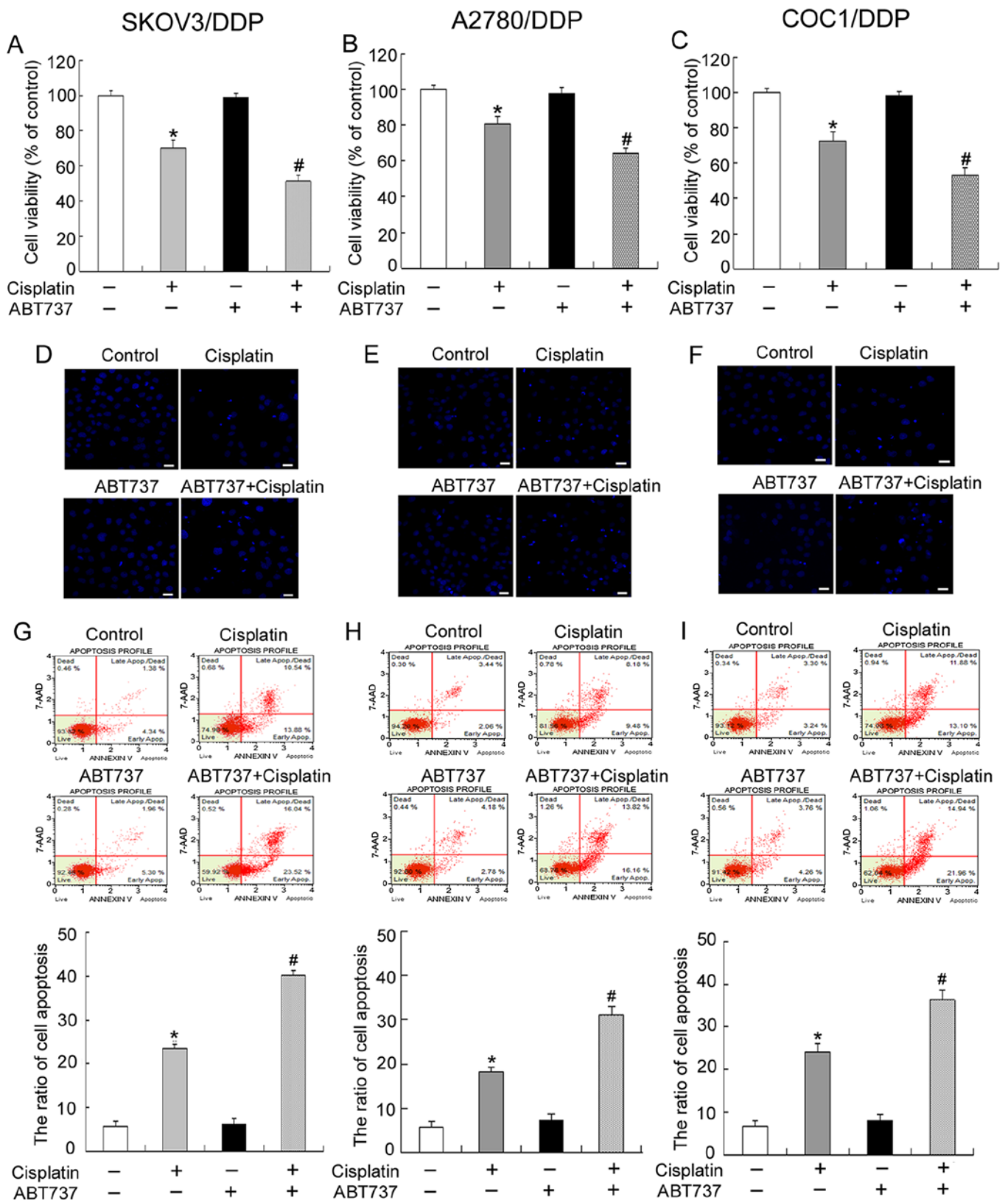
Figure 1. ABT737 increases cisplatin-induced growth inhibition and apoptosis in cisplatin-resistant ovarian cancer cells. (A-C) SKOV3/DDP, COC1/DDP and A2780/DDP cells were treated with 15 µg/ml cisplatin and/or 5 µM ABT737 for 24 h. Cell viability was determined by MTT assay. Data are presented as mean ± SD, n=3. *P<0.05 vs. control, #P<0.05 vs. cisplatin. (D-F) Cells were treated with 15 µg/ml cisplatin and/or 5 µM ABT737 for 24 h, and stained with Hoechst 33342. Cell morphology was observed by confocal microscopy (bar, 20 µm). (G-I) Apoptosis was assessed by staining for Annexin V and 7-AAD, and analysed by Muse cell analyser. Data are presented as mean ± SD, n=3. *P<0.05 vs. control, #P<0.05 vs. cisplatin.

COC1/DDP and A2780/DDP cells) with ABT737 in combination with cisplatin to investigate whether ABT737 would enhance the antitumor effects of cisplatin. On the basis of our previous studies (unpublished data), the non-toxic dose of
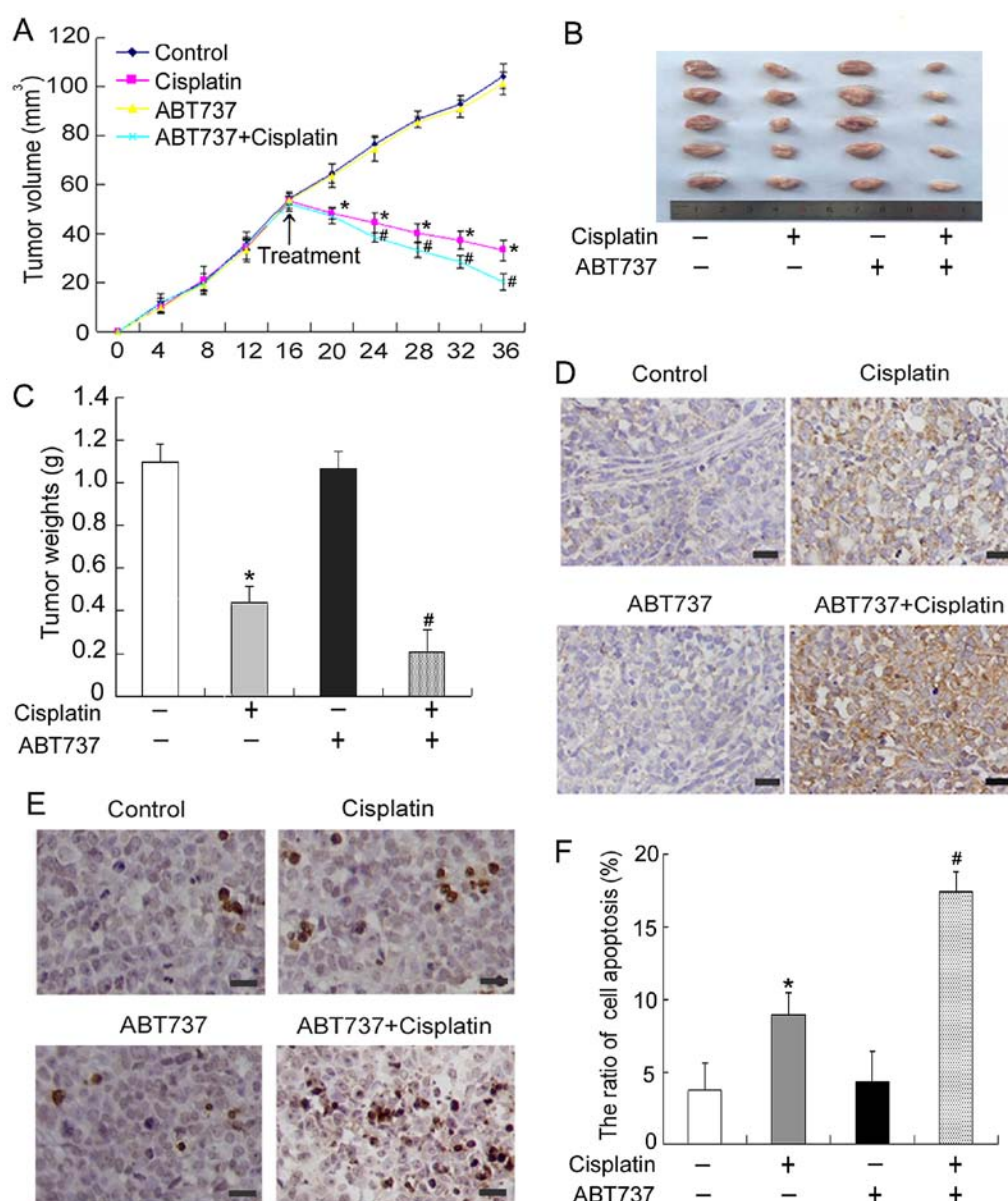
Figure 2. ABT737 and cisplatin have a synergistic effect in the treatment of human ovarian cancer xenograft mouse models. (A) Tumor volumes were measured every four days and tumor volumes calculated as described in Materials and methods. Data are presented as mean ± SD, n=3. *P<0.05 vs. control, #P<0.05 vs. cisplatin. (B) Tumors in mice were dissected and photographed at the end of 36 days. The images were captured showing tumor sizes for each group. (C) Comparison of the weights of excised tumors at the end of 36 days. Data are presented as mean ± SD, n=3. *P<0.05 vs. control, #P<0.05 vs. cisplatin. (D) Tissue sections were prepared from ovarian tumor tissue of nude mice at week 3 after treatment. The expression profile of cleaved caspase-3 was evaluated via an immunohistochemistry assay (scale bar, 50 μm). (E) Cancer samples were fixed in 4% PFA and paraffin-embedded. Cell apoptosis was measured by TUNEL assay (scale bar, 50 μm). (F) The quantification of apoptosis in the nude mouse xenograft model exposed to cisplatin and/or ABT737. Data are presented as mean ± SD, n=3. *P<0.05 vs. control, #P<0.05 vs. cisplatin.

ABT737 in SKOV3/DDP, COC1/DDP and A2780/DDP cells for 24 h is 5 μM. Thus, we treated SKOV3/DDP, COC1/DDP and A2780/DDP cells with 15 μg/ml cisplatin and/or 5 μM ABT737 for 24 h. MTT assays indicated that ABT737 increased cisplatin-induced growth inhibition (Fig. 1A-C).

On the basis of these results, we treated cells with cisplatin and/or ABT737 for 24 h and then examined apoptotic chromatin condensation with Hoechst 33342 staining. These results showed that ABT737 increased cisplatin-induced apoptotic chromatin condensation (Fig. 1D-F). Additionally, flow cytometry analysis revealed that the apoptosis rate was clearly higher in SKOV3/DDP, COC1/DDP and A2780/DDP cells exposed to cisplatin and ABT737 for 24 h compared

with cells treated with cisplatin alone (Fig. 1G-I). These results indicate that ABT737 restores sensitivity to cisplatin in cisplatin-resistant ovarian cancer cells.

ABT737 and cisplatin have a synergistic effect in the treatment of human ovarian cancer xenograft mouse models. After the *in vitro* experiments, *in vivo* experiments were performed to determine whether ABT737 contributes to suppressing tumor growth in combination with cisplatin. SKOV3/DDP cells were subcutaneously inoculated into BALB/c nude mice to establish a subcutaneous transplant tumor model. The tumor growth curve over time was recorded (Fig. 2A). As predicted, ABT737 plus cisplatin caused marked tumor growth inhibi-
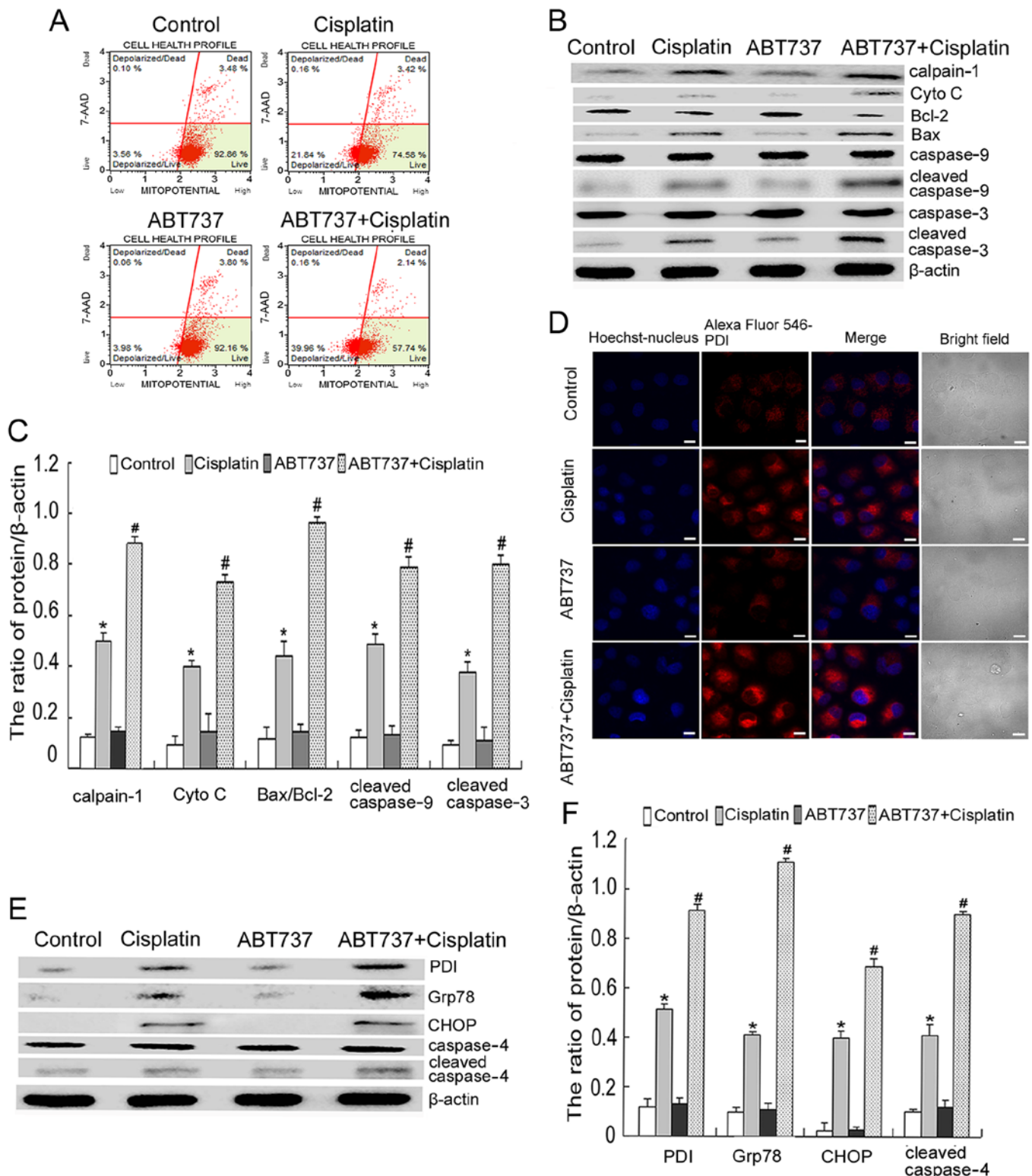
Figure 3. ABT737 enhances cisplatin-induced mitochondrial apoptosis and ER-mediated apoptosis in SKOV3/DDP cells. (A) SKOV3/DDP cells were treated with 15 µg/ml cisplatin and/or 5 µM ABT737 for 6 h. ΔΨm was assessed by staining for MitoPotential dye and 7-AAD, and analysed by Muse cell analyser. (B and C) SKOV3/DDP cells were treated with 15 µg/ml cisplatin and/or 5 µM ABT737 for 24 h. Western blot analysis for the expression of calpain-1, Cyto C, Bax, Bcl-2, cleaved caspase-9 and cleaved caspase-3 after normalization to β-actin and quantification. Data are presented as mean ± SD, n=3. *P<0.05 vs. control, #P<0.05 vs. cisplatin. (D) SKOV3/DDP cells were treated with 15 µg/ml cisplatin and/or 5 µM ABT737 for 24 h. Distribution of PDI was observed by confocal microscopy (bar, 10 µm). (E and F) SKOV3/DDP cells were treated with 15 µg/ml cisplatin and/or 5 µM ABT737 for 24 h. Western blot analysis for the expression of PDI, Grp78, CHOP and cleaved caspase-4 after normalization to β-actin and quantification. Data are presented as mean ± SD, n=3. *P<0.05 vs. control, #P<0.05 vs. cisplatin.

tion compared with treatment with cisplatin-only (Fig. 2B). The final tumor weights were 1.01, 0.39, 0.97 and 0.19 g for

BALB/c nude mice injected i.p. with NS, cisplatin, ABT737 or a combination treatment, respectively (Fig. 2C). Next, we
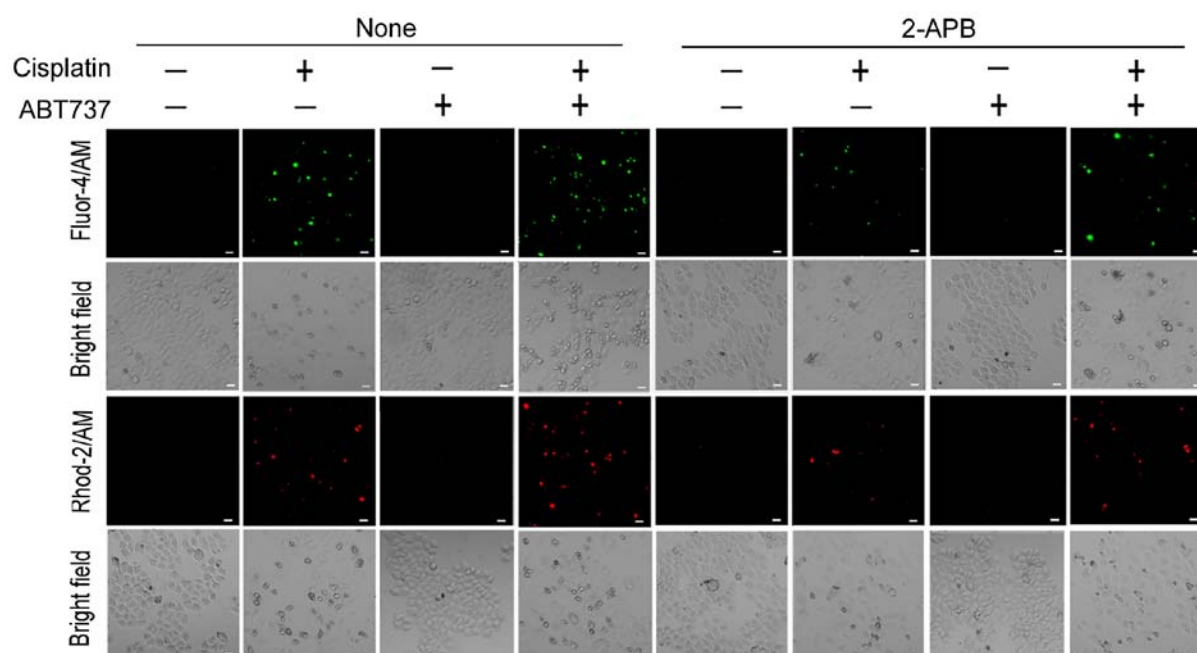
Figure 4. ABT737 increases cisplatin-induced Ca^{2+} transfer from the ER to the cytosol and mitochondria. SKOV3/DDP cells were treated with 15 μg/ml cisplatin, 5 μM ABT737, or both, in the presence or absence of 50 μM 2-APB for 24 h. Confocal microscopy was used to detect cytoplasmic and mitochondrial Ca^{2+} levels (scale bar, 20 μm).

used immunohistochemical methods to detect the expression of the apoptosis-related protein cleaved caspase-3 in mice exposed to cisplatin and/or ABT737 for 20 days. As shown in Fig. 2D, ABT737 combined with cisplatin treatment led to the upregulation of cleaved caspase-3 compared with treatment with cisplatin only. Furthermore, TUNEL assays were used to determine whether ABT737 had a synergistic effect with cisplatin in inducing cell apoptosis in mouse models of ovarian cancer. These results showed that the number of apoptotic cells in the cisplatin plus ABT737 group was significantly greater than that of the cisplatin group (Fig. 2E and F). Together, these data suggest that ABT737 and cisplatin have a synergistic effect in the treatment of human ovarian cancer xenograft mouse models.

ABT737 enhances cisplatin-induced mitochondrial apoptosis and ER-mediated apoptosis in SKOV3/DDP cells. First, we investigated whether ABT737 would enhance cisplatin-induced mitochondrial apoptosis. To determine the effect of cisplatin and/or ABT737 on mitochondrial function, we measured $\Delta\Psi$m by using flow cytometry after 6 h. As shown in Fig. 3A, the combination treatment further reduced the cisplatin-induced decrease of $\Delta\Psi$m. Moreover, western blot analysis showed that the combination treatment increased the ratio of Bax/Bcl-2 and enhanced the expression of mitochondrial apoptosis-related proteins (calpain-1, Cyto C, cleaved caspase-9 and cleaved caspase-3), as compared with the cisplatin treatment (Fig. 3B and C).

A growing body of research suggests that cisplatin triggers ER stress and induces ER stress-mediated apoptotic events (2). Hence, we further investigated whether ABT737 enhanced cisplatin-induced ER stress-mediated apoptosis in SKOV3/DDP cells. Using confocal microscopy, we found that ABT737 increased the expression of PDI induced by

cisplatin (Fig. 3D). We assessed the expression of ER stress-related proteins (PDI, Grp78, CHOP and cleaved caspase-4) by western blot analysis. These results showed that the combination treatment enhanced the expression of PDI, Grp78, CHOP and cleaved caspase-4, as compared with the cisplatin treatment (Fig. 3E and F). Thus, we demonstrated that the intrinsic mitochondrial apoptotic pathway and ER-mediated apoptosis are actively involved in the ABT737-mediated increase in the cytotoxic effects of cisplatin on SKOV3/DDP cells.

ABT737 increases cisplatin-induced Ca^{2+} transfer from the ER to the cytosol and mitochondria. Ca^{2+} is not only a key regulator of cell survival but also triggers cell apoptosis in response to various physiological and pathological conditions. A growing body of literature shows that cytoplasmic and mitochondrial Ca^{2+} overload can contribute to ER-mediated apoptosis and mitochondrial apoptosis (22,27). As described in Introduction, the ER is the most important Ca^{2+} storage compartment in eukaryotic cells. Therefore, we determined whether mitochondrial and cytoplasmic Ca^{2+} overload is a result of Ca^{2+} release from the ER. We used 2-APB, an IP3R antagonist that inhibits ER Ca^{2+} efflux (27). The fluorescent dyes Fluo-4/AM and Rhod-2/AM were used to detect cytoplasmic and mitochondrial Ca^{2+} levels in SKOV3/DDP cells, respectively. As shown in Fig. 4, the cytoplasmic and mitochondrial Ca^{2+} elevation induced by cisplatin or/and ABT737 in SKOV3/DDP cells was markedly reduced in the presence of 2-APB. These results strongly suggest that ABT737 increases cisplatin-induced Ca^{2+} transfer from the ER to the cytosol and mitochondria.

ABT737 enhances cisplatin-induced ER-mitochondria contacts in SKOV3/DDP cells. We showed that ABT737 enhanced cisplatin-increased mitochondrial Ca^{2+} levels in the previous experiments (Fig. 4). Therefore, we next explored
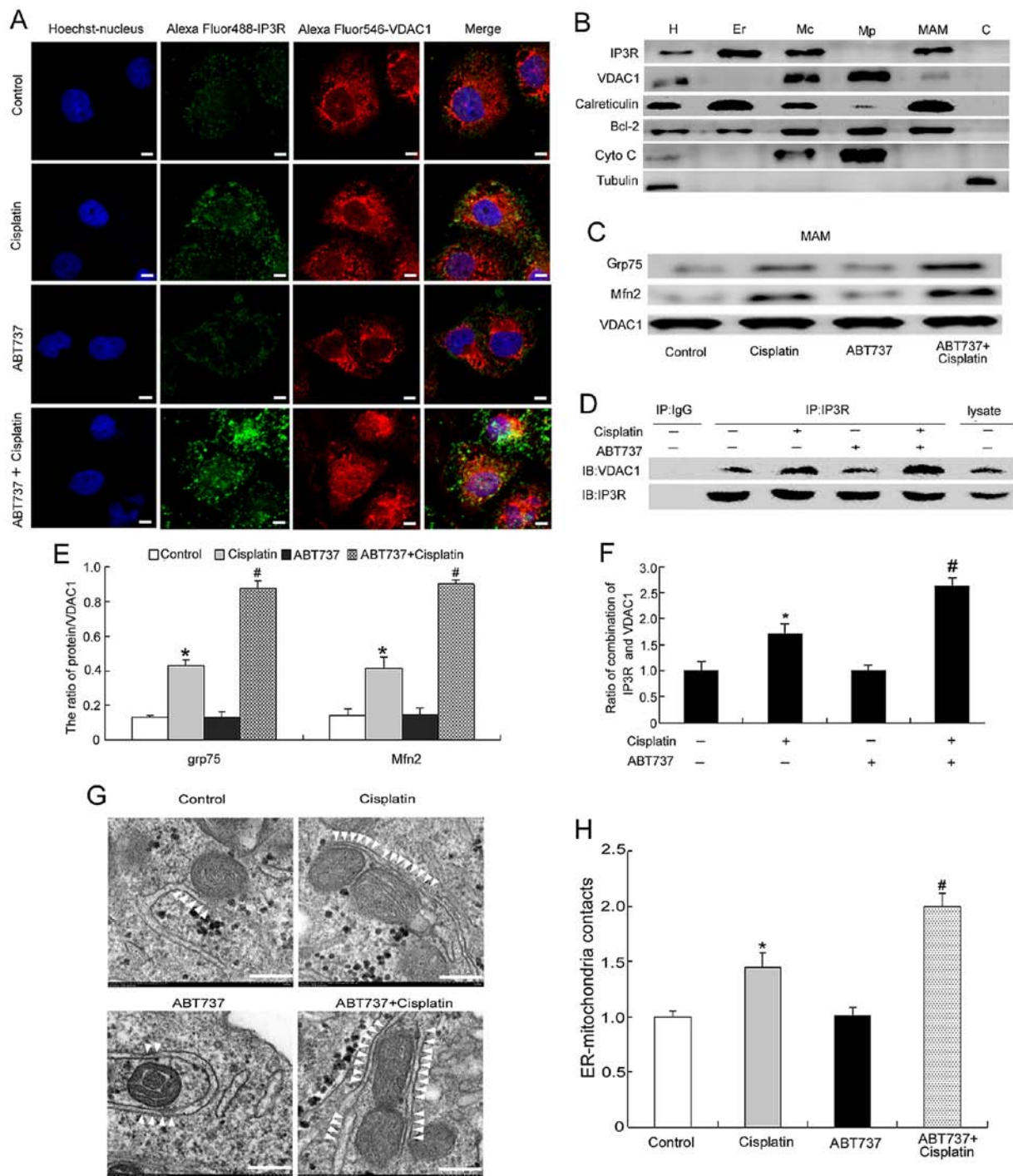
Figure 5. ABT737 enhances cisplatin-induced ER-mitochondria contacts in SKOV3/DDP cells. (A) Colocalization of IP3R and VDAC1 in SKOV3/DDP cells treated with 15 μg/ml cisplatin and/or 5 μM ABT737 for 24 h (bar, 5 μm). (B) Protein components of subcellular fractions prepared from SKOV3/DDP cells revealed by immunoblot analysis. H, homogenate; Mc, crude mitochondrial fraction; Mp, pure mitochondrial fraction; MAM, mitochondria-associated membrane. C, cytosol. (C and E) Analysis of Grp75 and Mfn2 at the MAM interface in SKOV3/DDP cells treated with cisplatin and/or ABT737 for 24 h. Data are presented as mean ± SD, n=3. *P<0.05 vs. control, #P<0.05 vs. cisplatin. (D and F) MAM fraction from SKOV3/DDP cells was subjected to immunoprecipitation with anti-IP3R antibody or normal IgG and then immunoblotted with anti-VDAC1 antibody. Lysate indicates the MAM fraction that was not subjected to immunoprecipitation. Data are presented as mean ± SD, n=3. *P<0.05 vs. control, #P<0.05 vs. cisplatin. (G) Representative transmission electron microscopy photomicrographs of SKOV3/DDP cells treated with cisplatin and/or ABT737 for 24 h (bar, 200 nm). White arrowheads indicate ER-mitochondria contacts. (H) Quantification of ER-mitochondria contacts of electron microscopy images. Data are presented as mean ± SD, n=3. *P<0.05 vs. control, #P<0.05 vs. cisplatin.

whether the increased mitochondrial Ca^{2+} levels were mediated by increasing the ER-mitochondria contact sites. IP3R and VDAC1 localize to the mitochondria and ER, respectively (13-15,28). We used confocal microscopy to analyze the co-localization of IP3R and VDAC1. The yellow areas represent co-localization between IP3R and VDAC1, and these results demonstrated that ABT737 enhanced cisplatin-induced ER-mitochondria contact sites (Fig. 5A).
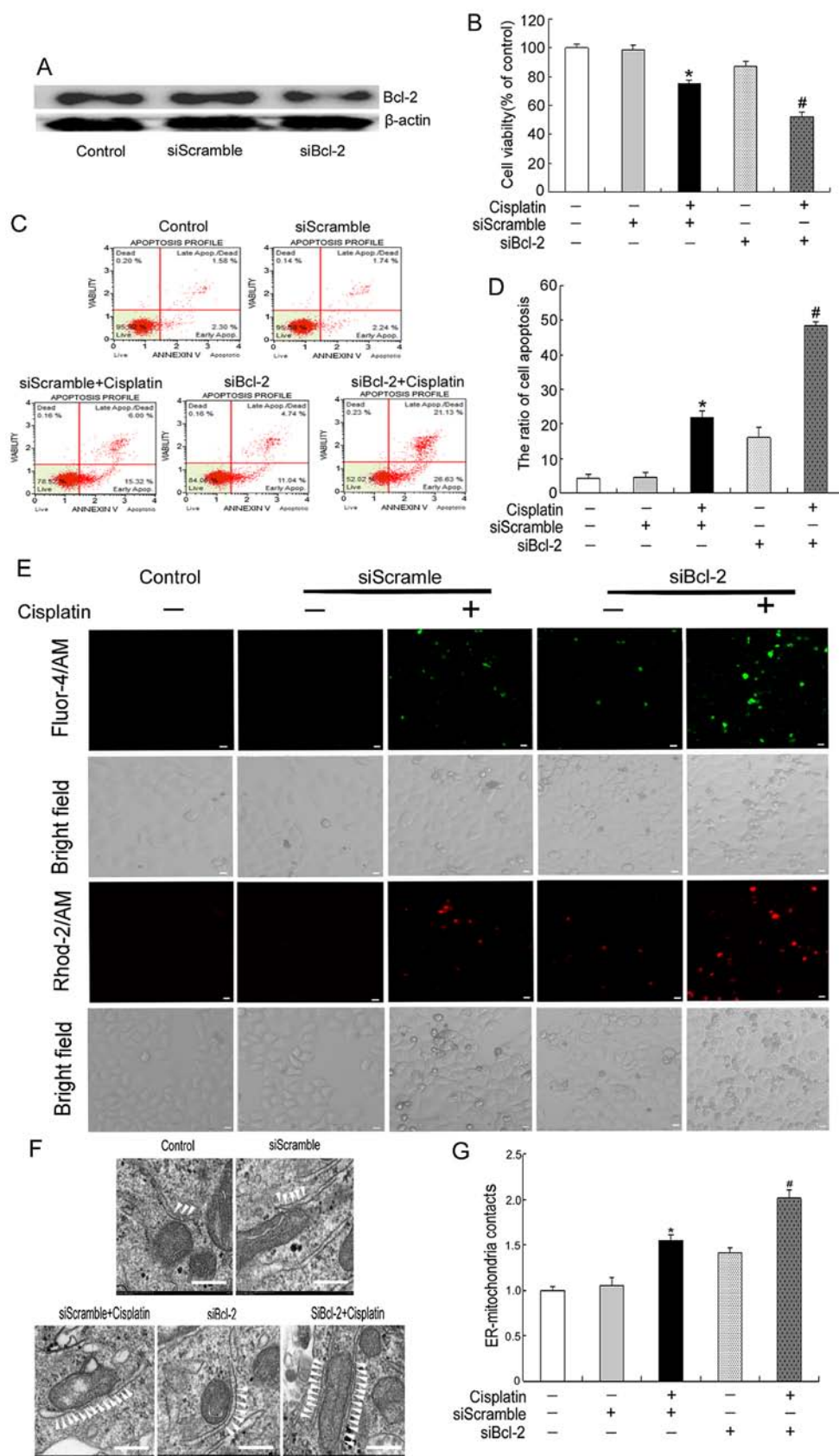
Figure 6. Bcl-2 siRNA increases sensitivity to cisplatin by increasing cytoplasmic and mitochondrial Ca^{2+} levels. SiBcl-2 increases sensitivity to cisplatin by decreasing Bcl-2 expression at ER and mitochondria. (A) Western blotting analysed the knockdown efficiency of Bcl-2, siScramle was used as negative control. (B) Cell viability was determined by MTT assay. Data are presented as mean ± SD, n=3. *P<0.05 vs. control, #P<0.05 vs. cisplatin plus siScramle group. (C) Apoptosis was assessed by staining for Annexin V and 7-AAD, and analysed by Muse cell analyser. (D) The quantification of apoptosis in SKOV3/DDP cells exposed to different treatment for 24 h. Data are presented as mean ± SD, n=3. *P<0.05 vs. control, #P<0.05 vs. cisplatin plus siScramle group. (E) Confocal microscopy was used to detect cytoplasmic and mitochondrial Ca^{2+} in cells exposed to different treatment for 24 h (scale bar, 10 μm). (F) Representative transmission electron microscopy photomicrographs of SKOV3/DDP cells exposed to different treatment for 24 h (bar, 200 nm). White arrowheads indicate ER-mitochondria contacts. (G) Quantification of ER-mitochondria contacts of electron microscopy images. Data are presented as mean ± SD, n= 3. *P<0.05 vs. control, #P<0.05 vs. cisplatin plus siScramle group.

Next, we detected the changes in the ER-mitochondria contact sites by western blotting and immunoprecipitation. Before studying the changes in ER-mitochondria interactions, we assessed the quality of each fraction by immunoblotting for subcellular organelle marker proteins: IP3R and calreticulin for the ER and MAM; VDAC1 for the mitochondria and MAM; Bcl-2 which enriches mitochondria and ER and is also present in MAM; Cyto C for the mitochondria; tubulin for the cytoplasm (17,24,28). As expected, the data showed that we obtained highly pure fractions, and there was no cross-contamination (Fig. 5B). By analyzing MAM composition, we found that ABT737 enhanced the cisplatin-induced interactions of VDAC1 with Grp75 and Mfn2 (Fig. 5C and E), thus suggesting that ER-mitochondria contact sites induced by cisplatin were enhanced in the combination treatment. Then, we treated cells with cisplatin and/or ABT737 for 24 h. The MAM fraction was immunoprecipitated using the anti-IP3R antibody followed by western blotting using the anti-VDAC1 antibody. These results showed that ABT737 enhanced the cisplatin-induced IP3R-VDAC1 interactions (Fig. 5D and F).

Finally, we used electron microscopy to examine the ultrastructural changes in MAM in the cisplatin and/or ABT737 group for 24 h. White arrowheads indicate the ER-mitochondria interactions. The contact points between the two organelles were significantly increased in the combination-treatment group compared with the control group (Fig. 5G and H). In summary, we concluded that ABT737 enhances cisplatin-induced mitochondrial Ca^{2+} levels by increasing ER-mitochondria contact sites.

Bcl-2 siRNA increases sensitivity to cisplatin by increasing cytoplasmic and mitochondrial Ca^{2+} levels. To better clarify the role of Bcl-2 in cisplatin resistance in SKOV3/DDP cells, we depleted the endogenous Bcl-2 using a specific siRNA in SKOV3/DDP cells and observed that the Bcl-2 protein expression was clearly downregulated (Fig. 6A). MTT assays showed that Bcl-2 siRNA combined with cisplatin for 24 h markedly decreased cell viability compared with that in the cisplatin plus siScramble group (Fig. 6B). Additionally, flow cytometry analysis revealed that the apoptosis rate was substantially higher in SKOV3/DDP cells exposed to cisplatin combined with Bcl-2 siRNA for 24 h compared with cells treated with cisplatin plus siScramble (Fig. 6C and D). Consistently with the results in Fig. 4, Bcl-2 siRNA also enhanced the cisplatin-induced cytoplasmic and mitochondrial Ca^{2+} elevations (Fig. 6E). Finally, we used electron microscopy to examine the ultrastructural changes of MAM after treatment with cisplatin and/or Bcl-2 siRNA. White arrowheads indicate the ER-mitochondria interactions. The contact points between the two organelles were significantly increased after the cisplatin plus Bcl-2 siRNA treatment for 24 h compared with the cisplatin plus siScramble treatment (Fig. 6F and G). Together, these findings suggest that Bcl-2 siRNA improves the sensitivity of ovarian cancer cells to cisplatin by increasing cytoplasmic and mitochondrial Ca^{2+} levels.

Discussion

Bcl-2 overexpression is recognized as one of the key mechanisms underlying tumor cell apoptosis escape and intrinsic or acquired cisplatin resistance (20,29,30). Hence, Bcl-2 has attracted considerable attention as a possible target for the treatment of cancer, including ovarian cancer. ABT-737, a small molecule compound, inhibits Bcl-2 by mimicking the function of the BH3-only protein (31-33). Using a xenograft model of hepatoblastoma (HB), Lieber *et al* have reported that ABT737 restores the cisplatin sensitivity of cisplatin-resistant HB cells and significantly decreases tumor growth, as compared with that observed after cisplatin monotherapy (34). Additionally, our previous results have shown that ABT737 enhances cisplatin-induced Bcl-2 downregulation and cisplatin-induced apoptosis through the regulation of mitochondrial dynamics in cholangiocarcinoma cells (25). In this study, ABT737 enhanced cisplatin-induced apoptotic chromatin condensation and cell apoptosis in cisplatin-resistant ovarian cancer cells (Fig. 1). To evaluate the effect of cisplatin combined with ABT737 on antitumor activity *in vivo*, a BALB/c nude mouse subcutaneous transplant tumor model was established using SKOV3/DDP cells. The results indicated that cisplatin combined with ABT737 had an additive inhibitory effect on tumorigenesis (Fig. 2).

An increasing number of studies have found that cisplatin is actively involved in mitochondria-mediated and ER-mediated apoptosis (35,36). Interestingly, Bcl-2 is predominantly located in the mitochondria and ER (30). Therefore, this finding suggests that ABT737 may increase the cytotoxic effects of cisplatin via the above two pathways. In this study, we found that ABT737 enhanced cisplatin-induced ΔΨm collapse and Cyto C release and increased the cisplatin-induced elevated Bax/Bcl-2 ratio and calpain-1, cleaved caspase-9, cleaved caspase-3 expression. Additionally, ABT737 increased Grp78, CHOP and cleaved caspase-4 induced by cisplatin (Fig. 3). All of our results demonstrate that ABT737 improved the response of SKOV3/DDP cells to cisplatin by mitochondria-mediated and ER-mediated apoptosis.

Ca^{2+}, a ubiquitous intracellular messenger, is a key determinant of cell function and survival. Altered Ca^{2+} homeostasis has an adverse effect on proliferating cells (37,38). A membrane-permeant inhibitor of IP3R, 2-APB, specifically inhibits IP3R-mediated Ca^{2+} release (39,40). Using 2-APB, Splettstoesser *et al* revealed that cisplatin-induced ER Ca^{2+} release results in programmed cell death due to activation of calpain (41). Calpain-1, a Ca^{2+}-dependent cysteine endopeptidase, can be activated by a small increase in cytoplasmic Ca^{2+} levels (10,42). Studies by Zheng *et al* and Altznauer *et al* and have shown that Ca^{2+}-induced calpain-1 triggers mitochondria-mediated and ER-mediated apoptosis (10,43). Recently, we showed that cisplatin increases cytosolic and mitochondrial Ca^{2+} levels, activates calpain-1, and eventually leads to mitochondria- and ER-mediated apoptosis (27). However, the effects of cisplatin plus ABT737 on intracellular Ca^{2+} signals have not been reported in the literature. In this study, to investigate the effect of cisplatin plus ABT737 on cytosolic and mitochondrial Ca^{2+} levels, we used the fluorescent dyes Fluo-4/AM and Rhod-2/AM to detect cytoplasmic and mitochondrial Ca^{2+} levels in SKOV3/DDP cells. Our experimental results showed that ABT737 increased cytoplasmic and mitochondrial Ca^{2+} levels induced by cisplatin and enhanced cisplatin-mediated calpain-1 activation, eventually leading to apoptosis (Figs. 3B and 4). These results indicate

that cytoplasmic and mitochondrial Ca^{2+} overload increased SKOV3/DDP cell sensitivity to cisplatin-induced cytotoxicity, thus possibly providing a new approach for treating cisplatin-resistant ovarian cancer.

The signaling mechanisms linking MAM and cancer cell apoptosis have attracted substantial interest (44-47) The phosphofurin acidic cluster sorting protein-2 (PACS-2), a cytosolic sorting protein, is required for the integrity of MAM (48). Using siRNA depletion of PACS-2, Simmen *et al* have demonstrated that low expression of PACS-2 blocks the apoptosis of STS-mediated human melanoma A7 cells, possibly through decreased transfer of Ca^{2+} from the ER to the mitochondria (48). Similarly, using fluorescence labeling of PDI (the marker protein of ER) and VDAC1 (the marker protein of mitochondria), our previous studies showned that cisplatin increases ER-mitochondria contacts, and this is followed by highly efficient transportation of Ca^{2+} from the ER to the mitochondria, ultimately resulting in mitochondrial Ca^{2+} overload and apoptosis in SKOV3 cells (12). Next, we determined whether the increase in mitochondrial Ca^{2+} levels induced by cisplatin and ABT737 is achieved through the increase in ER-mitochondrial cross-talk in SKOV3/DDP cells. In our study, through the fluorescence labeling of IP3R and VDAC1, we showed that ABT737 increased cisplatin-induced ER-mitochondria contacts. We analyzed MAM composition and found that ABT737 increased cisplatin-induced Grp75 and Mfn2 expression at the MAM interface. These results indicate that ABT737 increases cisplatin-induced ER-mitochondria interactions, a finding consistent with the results of electron microscopy (Fig. 5). All of these results suggest that enhanced ER-mitochondria coupling leads to mitochondrial Ca^{2+} overload and subsequent apoptosis by favoring Ca^{2+} transfer from the ER to the mitochondria. Interestingly, it has been reported that ER close to the mitochondria may sense local cytoplasmic Ca^{2+} increases, and the mitochondrial Ca^{2+} increase is closely coupled to the increase in cytoplasmic Ca^{2+} levels (49). Cytoplasmic Ca^{2+}-dependent calpain-1 activation is an important element of mitochondria-mediated and ER-mediated apoptosis. We suggest that increased ER-mitochondria contact sites allow for calpain-1-mediated apoptotic effects. However, further investigations are required to test this possibility.

To further explore whether the downregulation of Bcl-2 can increase the cytotoxic effects of cisplatin, we inhibited Bcl-2 expression by using siRNA transfection in SKOV3/DDP cells. Our study revealed that Bcl-2 siRNA enhanced the inhibitory effect of cisplatin on SKOV3/DDP cell proliferation and also enhanced cisplatin-induced apoptosis (Fig. 6B-D). Moreover, Bcl-2 knockdown significantly enhanced cisplatin-induced cytoplasmic and mitochondrial Ca^{2+} elevation and cisplatin-induced ER-mitochondria cross-talk in SKOV3/DDP cells (Fig. 6E-G). These results further indicated that increasing MAM formation plays a fundamental role in cell apoptosis by driving higher Ca^{2+} accumulation in the mitochondria.

In conclusion, in a departure from conventional therapeutic strategies for overcoming cisplatin resistance, we explored an alternative therapeutic strategy linking cisplatin resistance to Bcl-2-regulated Ca^{2+} signals in ovarian cancer cells. The pharmacological inhibition of Bcl-2 or Bcl-2 siRNA reversed the cisplatin resistance of SKOV3/DDP cells by increasing cisplatin-induced cytoplasmic and mitochondrial Ca^{2+} levels.

MAM not only promotes higher calcium transfer from the ER to the mitochondria, thus leading to mitochondrial Ca^{2+} overload, but also may allow for calpain-1-mediated apoptosis. Our experimental results elucidate the antitumor mechanism of Bcl-2 via MAM, suggesting a possibility for individualized treatment of ovarian cancer patients.

Acknowledgements

References

1. Ma L, Xu Y, Su J, Yu H, Kang J, Li H, Li X, Xie Q, Yu C, Sun L, *et al*: Autophagic flux promotes cisplatin resistance in human ovarian carcinoma cells through ATP-mediated lysosomal function. Int J Oncol 47: 1890-1900, 2015.
2. Xu Y, Yu H, Qin H, Kang J, Yu C, Zhong J, Su J, Li H and Sun L: Inhibition of autophagy enhances cisplatin cytotoxicity through endoplasmic reticulum stress in human cervical cancer cells. Cancer Lett 314: 232-243, 2012.
3. Ferri KF and Kroemer G: Organelle-specific initiation of cell death pathways. Nat Cell Biol 3: E255-E263, 2001.
4. van Vliet AR, Verfaillie T and Agostinis P: New functions of mitochondria associated membranes in cellular signaling. Biochim Biophys Acta 1843: 2253-2262, 2014.
5. Farooqi AA, Li KT, Fayyaz S, Chang YT, Ismail M, Liaw CC, Yuan SS, Tang JY and Chang HW: Anticancer drugs for the modulation of endoplasmic reticulum stress and oxidative stress. Tumour Biol 36: 5743-5752, 2015.
6. Krebs J, Agellon LB and Michalak M: Ca(2+) homeostasis and endoplasmic reticulum (ER) stress: An integrated view of calcium signaling. Biochem Biophys Res Commun 460: 114-121, 2015.
7. Moretti D, Del Bello B, Allavena G and Maellaro E: Calpains and cancer: Friends or enemies? Arch Biochem Biophys 564: 26-36, 2014.
8. Huang Y, Li X, Wang Y, Wang H, Huang C and Li J: Endoplasmic reticulum stress-induced hepatic stellate cell apoptosis through calcium-mediated JNK/P38 MAPK and Calpain/Caspase-12 pathways. Mol Cell Biochem 394: 1-12, 2014.
9. Martinez JA, Zhang Z, Svetlov SI, Hayes RL, Wang KK and Larner SF: Calpain and caspase processing of caspase-12 contribute to the ER stress-induced cell death pathway in differentiated PC12 cells. Apoptosis 15: 1480-1493, 2010.
10. Zheng D, Wang G, Li S, Fan GC and Peng T: Calpain-1 induces endoplasmic reticulum stress in promoting cardiomyocyte apoptosis following hypoxia/reoxygenation. Biochim Biophys Acta 1852: 882-892, 2015.
11. Fonteriz RI, de la Fuente S, Moreno A, Lobatón CD, Montero M and Alvarez J: Monitoring mitochondrial [Ca(2+)] dynamics with rhod-2, ratiometric pericam and aequorin. Cell Calcium 48: 61-69, 2010.
12. Xu Y, Wang C, Su J, Xie Q, Ma L, Zeng L, Yu Y, Liu S, Li S, Li Z, *et al*: Tolerance to endoplasmic reticulum stress mediates cisplatin resistance in human ovarian cancer cells by maintaining endoplasmic reticulum and mitochondrial homeostasis. Oncol Rep 34: 3051-3060, 2015.
13. Anelli T, Bergamelli L, Margittai E, Rimessi A, Fagioli C, Malgaroli A, Pinton P, Ripamonti M, Rizzuto R and Sitia R: Eroiα regulates Ca(2+) fluxes at the endoplasmic reticulum-mitochondria interface (MAM). Antioxid Redox Signal 16: 1077-1087, 2012.
14. Hayashi T, Rizzuto R, Hajnoczky G and Su TP: MAM: More than just a housekeeper. Trends Cell Biol 19: 81-88, 2009.
15. Ouyang YB and Giffard RG: ER-mitochondria crosstalk during cerebral ischemia: Molecular chaperones and ER-mitochondrial calcium transfer. Int J Cell Biol 2012: 493934, 2012.
16. Rowland AA and Voeltz GK: Endoplasmic reticulum-mitochondria contacts: Function of the junction. Nat Rev Mol Cell Biol 13: 607-625, 2012.

17. Wieckowski MR, Giorgi C, Lebiedzinska M, Duszynski J and Pinton P: Isolation of mitochondria-associated membranes and mitochondria from animal tissues and cells. Nat Protoc 4: 1582-1590, 2009.
18. Paillard M, Tubbs E, Thiebaut PA, Gomez L, Fauconnier J, Da Silva CC, Teixeira G, Mewton N, Belaidi E, Durand A, et al: Depressing mitochondria-reticulum interactions protects cardio-myocytes from lethal hypoxia-reoxygenation injury. Circulation 128: 1555-1565, 2013.
19. Guo X, Chen KH, Guo Y, Liao H, Tang J and Xiao RP: Mitofusin 2 triggers vascular smooth muscle cell apoptosis via mitochondrial death pathway. Circ Res 101: 1113-1122, 2007.
20. Leisching G, Loos B, Botha M and Engelbrecht AM: Bcl-2 confers survival in cisplatin treated cervical cancer cells: Circumventing cisplatin dose-dependent toxicity and resistance. J Transl Med 13: 328, 2015.
21. Liu N, Xu Y, Sun JT, Su J, Xiang XY, Yi HW, Zhang ZC and Sun LK: The BH3 mimetic S1 induces endoplasmic reticulum stress-associated apoptosis in cisplatin-resistant human ovarian cancer cells although it activates autophagy. Oncol Rep 30: 2677-2684, 2013.
22. Scorrano L, Oakes SA, Opferman JT, Cheng EH, Sorcinelli MD, Pozzan T and Korsmeyer SJ: BAX and BAK regulation of endo-plasmic reticulum Ca^{2+}: A control point for apoptosis. Science 300: 135-139, 2003.
23. Giorgi C, Missiroli S, Patergnani S, Duszynski J, Wieckowski MR and Pinton P: Mitochondria-associated membranes: Composition, molecular mechanisms, and physiopathological implications. Antioxid Redox Signal 22: 995-1019, 2015.
24. Meunier J and Hayashi T: Sigma-1 receptors regulate Bcl-2 expression by reactive oxygen species-dependent transcriptional regulation of nuclear factor kappaB. J Pharmacol Exp Ther 332: 388-397, 2010.
25. Fan Z, Yu H, Cui N, Kong X, Liu X, Chang Y, Wu Y, Sun L and Wang G: ABT737 enhances cholangiocarcinoma sensitivity to cisplatin through regulation of mitochondrial dynamics. Exp Cell Res 335: 68-81, 2015.
26. Han W, Li L, Qiu S, Lu Q, Pan Q, Gu Y, Luo J and Hu X: Shikonin circumvents cancer drug resistance by induction of a necroptotic death. Mol Cancer Ther 6: 1641-1649, 2007.
27. Shen L, Wen N, Xia M, Zhang YU, Liu W, Xu YE and Sun L: Calcium efflux from the endoplasmic reticulum regulates cisplatin-induced apoptosis in human cervical cancer HeLa cells. Oncol Lett 11: 2411-2419, 2016.
28. Lee GH, Lee HY, Li B, Kim HR and Chae HJ: Bax inhibitor-1-mediated inhibition of mitochondrial Ca^{2+} intake regulates mitochondrial permeability transition pore opening and cell death. Sci Rep 4: 5194, 2014.
29. Tóthová E, Fricova M, Stecová N, Kafková A and Elbertová A: High expression of Bcl-2 protein in acute myeloid leukemia cells is associated with poor response to chemotherapy. Neoplasma 49: 141-144, 2002.
30. Akl H, Vervloessem T, Kiviluoto S, Bittremieux M, Parys JB, De Smedt H and Bultynck G: A dual role for the anti-apoptotic Bcl-2 protein in cancer: Mitochondria versus endoplasmic reticulum. Biochim Biophys Acta 1843: 2240-2252, 2014.
31. Zhang H, Zhong X, Zhang X, Shang D, Zhou YI and Zhang C: Enhanced anticancer effect of ABT-737 in combination with naringenin on gastric cancer cells. Exp Ther Med 11: 669-673, 2016.
32. Antignani A, Sarnovsky R and FitzGerald DJ: ABT-737 promotes the dislocation of ER luminal proteins to the cytosol, including pseudomonas exotoxin. Mol Cancer Ther 13: 1655-1663, 2014.
33. Gardner EE, Connis N, Poirier JT, Cope L, Dobromilskaya I, Gallia GL, Rudin CM and Hann CL: Rapamycin rescues ABT-737 efficacy in small cell lung cancer. Cancer Res 74: 2846-2856, 2014.
34. Lieber J, Dewerth A, Wenz J, Kirchner B, Eicher C, Warmann SW, Fuchs J and Armeanu-Ebinger S: Increased efficacy of CDDP in a xenograft model of hepatoblastoma using the apoptosis sensi-tizer ABT-737. Oncol Rep 29: 646-652, 2013.
35. Gatti L, Cassinelli G, Zaffaroni N, Lanzi C and Perego P: New mechanisms for old drugs: Insights into DNA-unrelated effects of platinum compounds and drug resistance determinants. Drug Resist Updat 20: 1-11, 2015.
36. Cullen KJ, Yang Z, Schumaker L and Guo Z: Mitochondria as a critical target of the chemotheraputic agent cisplatin in head and neck cancer. J Bioenerg Biomembr 39: 43-50, 2007.
37. Greenberg B, Butler J, Felker GM, Ponikowski P, Voors AA, Desai AS, Barnard D, Bouchard A, Jaski B, Lyon AR, et al: Calcium upregulation by percutaneous administration of gene therapy in patients with cardiac disease (CUPID 2): A randomised, multinational, double-blind, placebo-controlled, phase 2b trial. Lancet 387: 1178-1186, 2016.
38. Mattson MP and Chan SL: Calcium orchestrates apoptosis. Nat Cell Biol 5: 1041-1043, 2003.
39. Amcheslavsky A, Safrina O and Cahalan MD: State-dependent block of Orai3 TM1 and TM3 cysteine mutants: Insights into 2-APB activation. J Gen Physiol 143: 621-631, 2014.
40. Lee HC, Yoon SY, Lykke-Hartmann K, Fissore RA and Carvacho I: TRPV3 channels mediate Ca^{2+} influx induced by 2-APB in mouse eggs. Cell Calcium 59: 21-31, 2016.
41. Splettstoesser F, Florea AM and Büsselberg D: IP(3) receptor antagonist, 2-APB, attenuates cisplatin induced Ca^{2+}-influx in HeLa-S3 cells and prevents activation of calpain and induction of apoptosis. Br J Pharmacol 151: 1176-1186, 2007.
42. Villalpando Rodriguez GE and Torriglia A: Calpain 1 induce lysosomal permeabilization by cleavage of lysosomal associated membrane protein 2. Biochim Biophys Acta 1833: 2244-2253, 2013.
43. Altznauer F, Conus S, Cavalli A, Folkers G and Simon HU: Calpain-1 regulates Bax and subsequent Smac-dependent caspase-3 activation in neutrophil apoptosis. J Biol Chem 279: 5947-5957, 2004.
44. Giorgi C, De Stefani D, Bononi A, Rizzuto R and Pinton P: Structural and functional link between the mitochondrial network and the endoplasmic reticulum. Int J Biochem Cell Biol 41: 1817-1827, 2009.
45. Marchi S, Patergnani S and Pinton P: The endoplasmic retic-ulum-mitochondria connection: One touch, multiple functions. Biochim Biophys Acta 1837: 461-469, 2014.
46. López-Crisosto C, Bravo-Sagua R, Rodriguez-Peña M, Mera C, Castro PF, Quest AF, Rothermel BA, Cifuentes M and Lavandero S: ER-to-mitochondria miscommunication and metabolic diseases. Biochim Biophys Acta 1852A: 2096-2105, 2015.
47. Raturi A and Simmen T: Where the endoplasmic reticulum and the mitochondrion tie the knot: The mitochondria-associated membrane (MAM). Biochim Biophys Acta 1833: 213-224, 2013.
48. Simmen T, Aslan JE, Blagoveshchenskaya AD, Thomas L, Wan L, Xiang Y, Feliciangeli SF, Hung CH, Crump CM and Thomas G: PACS-2 controls endoplasmic reticulum-mitochon-dria communication and Bid-mediated apoptosis. EMBO J 24: 717-729, 2005.
49. Hajnóczky G, Davies E and Madesh M: Calcium signaling and apoptosis. Biochem Biophys Res Commun 304: 445-454, 2003.